Inorganic Chemistry

Article

pubs.acs.org/IC

Magnetic Structures of Heterometallic M(II)−M(III) Formate Compounds

Lidia Mazzuca,[†] Laura Cañadillas-Delgado,[‡] J. Alberto Rodríguez-Velamazán,[†,§] Oscar Fabelo,*[,†] Marco Scarrozza,[△] Alessandro Stroppa,[∥] Silvia Picozzi,[△] Jiong-Peng Zhao,[⊥] Xian-He Bu,*[,⊥] and Juan Rodríguez-Carvajal*[,†]

[†]Institut Laue-Langevin, 71 Avenue des Martyrs, CS 20156, 38042 Grenoble Cedex 9, France

[‡]Centro Universitario de la Defensa de Zaragoza, Ctra Huesca s/n, Zaragoza 50090, Spain

[§]Instituto de Ciencia de Materiales de Aragón, CSIC-Universidad de Zaragoza, C/Pedro Cerbuna 12, E-50009 Zaragoza, Spain

[∥]Consiglio Nazionale delle Ricerche, Istituto CNR-SPIN, UOS L'Aquila, 67100 L'Aquila, Italy

[⊥]Department of Chemistry and TKL of Metal and Molecule-Based Material Chemistry, Nankai University, Tianjin 300071, China

[△]Consiglio Nazionale delle Ricerche, Istituto CNR-SPIN, Sede Temporanea di Chieti, 66100 Chieti, Italy

Supporting Information

ABSTRACT: A study of the magnetic structure of the $[NH_2(CH_3)_2]_n[Fe^{III}M^{II}(HCOO)_6]_n$ niccolite-like compounds, with M^{II} = Co^{II} (**2**) and Mn^{II} (**3**) ions, has been carried out using neutron diffraction and compared with the previously reported Fe^{II}-containing compound (**1**). The inclusion of two different metallic atoms into the niccolite-like structure framework leads to the formation of isostructural compounds with very different magnetic behaviors due to the compensation or not of the different spins involved in each lattice. Below T_N, the magnetic order in these compounds varies from ferrimagnetic behavior for **1** and **2** to an antiferromagnetic behavior with a weak spin canting for **3**. Structure refinements of **2** and **3** at low temperature (45 K) have been carried out combining synchrotron X-ray and high-resolution neutron diffraction in a multipattern approach. The magnetic structures have been determined from the difference patterns between the neutron data in the paramagnetic and the magnetically ordered regions. These difference patterns have been analyzed using a simulated annealing protocol and symmetry analysis techniques. The obtained magnetic structures have been further rationalized by means of ab initio DFT calculations. The direction of the magnetic moment of each compound has been determined. The easy axis of the M^{II} for compound **1** (Fe^{II}) is along the *c* axis; for compound **2** (Co^{II}), the moments are mainly within the *ab* plane; finally, for compound **3** (Mn^{II}), the calculations show that the moments have components both in the *ab* plane and along the *c* axis.

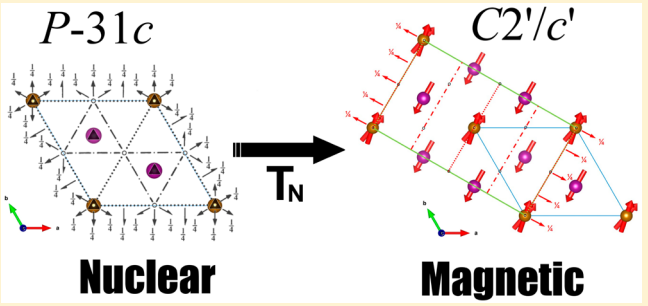

INTRODUCTION

The investigation of magneto−structural correlations of metal−organic networks has become the focus of intense research since their hybrid characteristics, stemming from metal cations and organic ligands, open countless possibilities for the creation of new smart materials.[1] Carboxylate ligands are ubiquitous in the design and synthesis of complexes with the desirable magnetic properties, since they are good candidates as mediators of local interactions between paramagnetic metal centers. Within this group of ligands, formate is the smallest carboxylate bridging ligand and is extensively used to construct molecular magnetic materials.[2] This ligand can be used to achieve not only zero-dimensional clusters but also higher dimensional structures, presenting multiple bridging modes able to mediate magnetic coupling efficiently.[3] These coordination modes generally determine the magnetic coupling between the connected paramagnetic centers. A common formate 3D structure is the niccolite-like metal organic framework, with a dense metal network where the formate groups act as bis-monodentate in an anti−anti coordination mode which mediates ferro- or antiferromagnetic coupling between neighboring spin carriers.[4] Magnetic properties become more diverse in heterometallic systems, since the combination of two or more magnetic centers in the same structure can lead to long-range magnetic order with ferrimagnetic behavior or with canted-antiferromagnetism, depending on the spins involved.

Among the possible magnetic metals, iron is a particularly interesting candidate for the design of molecule magnets because of its multivalence and different spin states.[5] Previous studies on $[NH_2(CH_3)_2]_n[Fe^{III}Fe^{II}(HCOO)_6]_n$ (**1**) have shown magnetic and electric ordering at low temperatures.[4a−c] A structural phase transition at 155 K seems to be related with the electric ordering, while the magnetic order appears at 37 K. The magnetic order

Received: August 5, 2016

DOI: 10.1021/acs.inorgchem.6b01866
Inorg. Chem. XXXX, XXX, XXX−XXX

consists of a weakly noncollinear ferrimagnetic structure where the Fe^{II} and the Fe^{III} ions are coupled antiferromagnetically. On the basis of this previous work we continued with the studies of $Fe^{III}M^{II}$ formate heterometallic frameworks. We focused in the combination of Co^{II} and Mn^{II} ions with the Fe^{III} centers, which is attractive because of the flexibility of these ions in adopting different coordination environments, together with the large single-ion anisotropy of the Co^{II} atom in contrast with the isotropy of the Mn^{II} ion.[6]

The present work is dedicated to two formate-based heterometallic compounds $[NH_2(CH_3)_2]_n[Fe^{III}M^{II}(HCOO)_6]_n$, with $M^{II} = Co^{II}$ (**2**) and $M^{II} = Mn^{II}$ (**3**). The structures and magnetic properties of these compounds have been determined previously using single-crystal X-ray diffraction and SQUID magnetometry, respectively.[4b] They are isomorphs to the previous $[NH_2(CH_3)_2]_n[Fe^{III}Fe^{II}(HCOO)_6]_n$ compound; however, we have seen that compounds **2** and **3** do not present structural transitions that could be associated with a change in their electrical properties. Both **2** and **3** crystallize in the *P*-31*c* space group and present a 3D niccolite topology (with perovskite tolerance factor α = 0.81 and 0.80 for **2** and **3**, respectively)[7] built up from a single crystallographically independent formate ligand which links Fe^{III} and M^{II} ions ($M^{II} = Co^{II}$(**2**) and Mn^{II}(**3**)) in an anti−anti manner. The cavities of the structures are filled with dimethylammonium cations $[NH_2(CH_3)_2]^+$, achieving the electroneutrality of the network (see Figure 1). The magnetic properties of **2** and **3** are also different from those of **1**: compound **2** shows ferrimagnetic behavior, while compound **3** presents a small spin-canting signal.

Herein we used ab initio calculations together with X-ray synchrotron single-crystal diffraction and neutron powder diffraction techniques to elucidate the occurrence and evolution of the different long-range magnetic orderings present in these compounds.

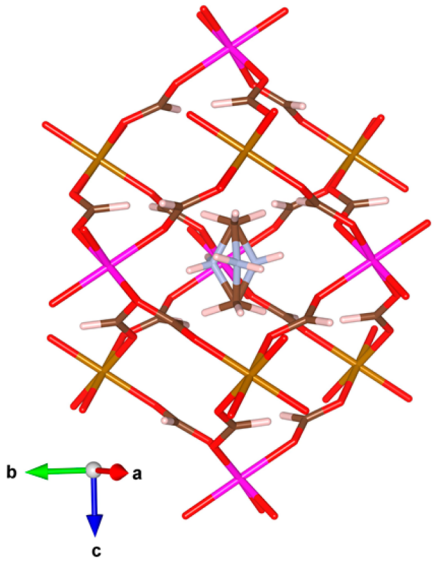

Figure 1. Detail of the crystal structure of the $[NH_2(CH_3)_2]_n[Fe^{III}M^{II}(HCOO)_6]_n$ niccolite-like compound [with $M^{II} = Fe^{II}$(**1**), Co^{II} (**2**), and Mn^{II} (**3**) ions]. $[NH_2(CH_3)_2]^+$ counterion is disordered into three different positions due to the 3-fold axis running through the carbon atoms of the methyl groups. The three possible positions within the $[Fe^{III}M^{II}(HCOO)_6]$ framework have been represented simultaneously. M^{II}, Fe^{III}, oxygen, nitrogen, carbon, and hydrogen atoms are represented in pink, gold, red, light blue, brown, and gray, respectively.

EXPERIMENTAL SECTION

Single-Crystal X-ray Structure Refinement. Data collection of compounds **2** and **3** was carried out by using synchrotron radiation with λ = 0.66951 Å at the CRISTAL beamline at SOLEIL synchrotron (Saclay, France) at 30, 45, 55, 65, 75, 85, 95, and 105 K using a He-cryostream (see Tables S1−S4). The wavelength was refined using a standard ruby sample, while the instrument model was refined at each temperature using the collected data. The data were indexed, integrated, and scaled using the CrysAlis PRO software program.[8] The structures of **2** and **3** were solved by direct methods using the SHELXS program. All non-hydrogen atoms were refined anisotropically by full-matrix least-squares technique based on F^2 using SHELXL.[9] The hydrogen atom of the formate ligand was positioned geometrically and refined using the difference electron density map. The final geometrical calculations and the graphical manipulations were carried out with PARST9,[10] PLATON,[11] and VESTA[12] programs.

Neutron Diffraction Measurements. Neutron powder diffraction experiments were performed on the high-intensity diffractometer D1B and on the high-resolution diffractometer D2B, both equipped with variable-temperature environment, at the Institut Laue Langevin (Grenoble, France). The samples were contained in a 6 mm cylindrical vanadium can and placed inside an Orange Cryostat. In order to obtain an accurate crystal structure of both compounds, diffraction patterns were acquired at 45 K at D2B (λ = 1.595 Å). The measurements at D1B were recorded using a λ = 2.521 Å wavelength, above and below the magnetic order temperature, at 45 and 2 K, respectively, with the aim of obtaining the magnetic structure of **2** and **3**. Moreover, thermodiffractograms between 2 and 45 K, at a heating rate of 0.1 K/min, were measured. Data reduction was carried out using LAMP software,[13] while the data refinement and calculations were carried out using the FullProf program suite.[14] A joint refinement (multipattern fit) of the synchrotron single-crystal and neutron powder diffraction data was carried out to determine the contribution of the light atoms and discard any structural phase transition related with the order of the hydrogen atoms (see Figure 2 and Figure S1). Magnetic structure models were deduced from the output of the BasIreps program included in the FullProf Suite.[15]

Density Functional Theory Calculations. All DFT calculations[16] were performed using the generalized gradient approximation to exchange-correlation functional according to Perdew−Becke−Erzenhof (PBE).[17] The electronic structure is computed using the projector augmented wave method (PAW),[18] as implemented in the Vienna ab initio simulation package (VASP).[19] The energy cutoff was set to 400 eV and a sampling grid of 4 × 4 × 2 Monkhorst−Pack grid of *k* points. The GGA + U[20] calculations within Dudarev's approach[21] were performed with 3 and 5 eV *U* values for Fe^{III}, Mn^{II}, and Co^{II}. For the calculation we considered the high-temperature structure for the three compounds. Since the counterion molecule is disordered over three possible local configurations, we selected an ordered arrangement of molecular dimethylammonium counterions compatible with an antiferroelectric arrangement. This will not change our discussions as far as the magnetic properties are concerned.

RESULTS AND DISCUSSION

Nuclear Structures. Although the crystal structures of **2** and **3** have been reported before, a brief structural description has been included hereafter in order to facilitate the understanding of their magnetic properties. Their structures consist of three-dimensional networks where each Fe^{III} ion is connected to six M^{II} ions [Co^{II} (**2**) and Mn^{II} (**3**)] by means of formate ligands in anti−anti conformation, forming an octahedral arrangement. In the same way, each M^{II} ion is surrounded by six Fe^{III} ions, and then each formate ligand always connects ions with different valence (see Figure 3).

The anionic framework is filled with dimethylammonium cations. The dimethylammonium cations are occupying an empty space of ca. 235.9 $Å^3$ for **2** and 239.9 $Å^3$ for **3**, corresponding to

DOI: 10.1021/acs.inorgchem.6b01866
Inorg. Chem. XXXX, XXX, XXX−XXX

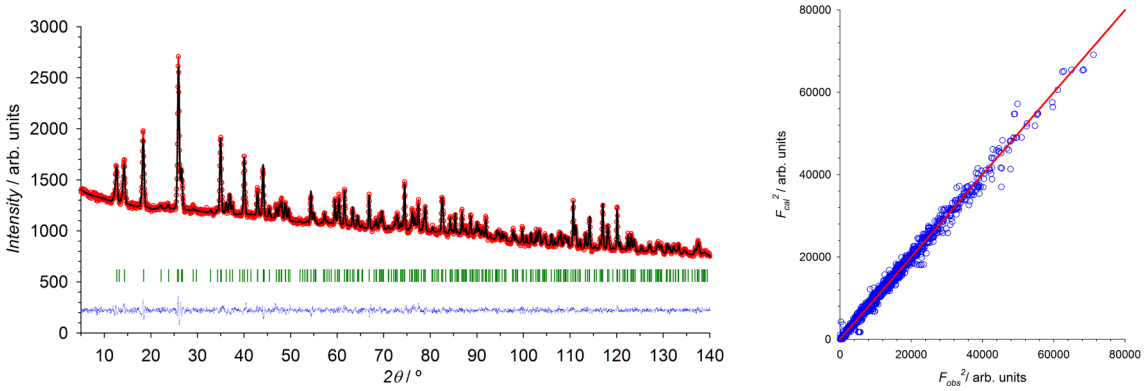

Figure 2. (Left) Experimental (open red circles) neutron powder diffraction data and calculated Rietveld refinement (black solid line) pattern for $[NH_2(CH_3)_2]_n[Fe^{III}Co^{II}(HCOO)_6]_n$ compound (data collected at 45 K using the D2B instrument with λ= 1.59465 Å). The difference between observed and calculated patterns has been represented in blue. Vertical green marks represent the position of the Bragg reflections. (Right) Plot of the observed vs calculated square structure factors collected, corresponding to the data collected at 45 K at the CRISTAL beamline. Experimental data are represented as open blue circles, and the ideal case ($F_{cal}^2 = F_{obs}^2$) is represented as a solid red line. Refinement has been done in the space group *P*-31*c* with the associated cell parameters $a = b = 8.22225(6)$ Å, $c = 13.68859(16)$ Å, $\alpha = \beta = 90°$, and $\gamma = 120°$. Multipattern data refinement gives the following agreement factors $\chi^2 = 2.03$ and R_B= 7.09% for neutron and R_F = 5.75% for X-ray data.

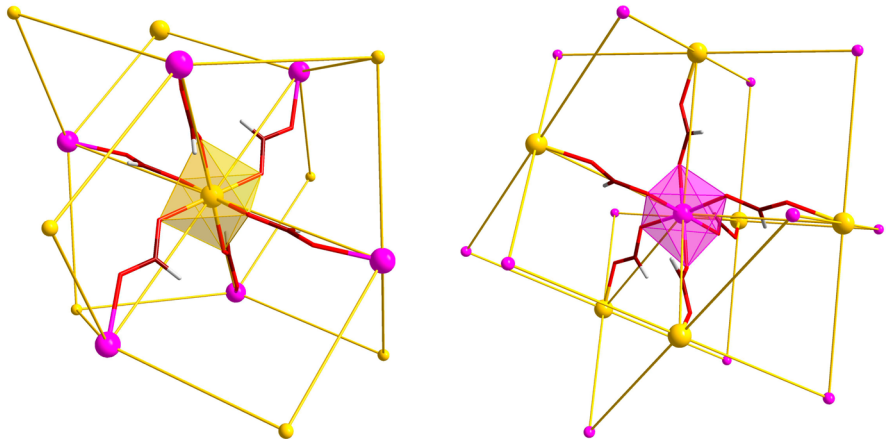

Figure 3. Detailed view of the niccolite structural network topology together with detail of the Fe^{III} (left) and M^{II} environment (right). The topology in the Schläfly notation corresponds with a bimodal network $(4^{12}\cdot6^3)\cdot(4^9\cdot6^6)$, where the Fe^{III} ions lay on the $(4^{12}\cdot6^3)$ node and the M^{II} site is placed on the $(4^9\cdot6^6)$ node. M^{II}, Fe^{III}, oxygen, carbon, and hydrogen atoms are represented in pink, gold, red, brown, and gray, respectively.

29.5% and 29.1% of the unit cell volume. The remaining empty space considering the dimethylammonium counterions is ca. 14.5 $Å^3$ for **2** and 14.1 $Å^3$ for **3**, corresponding to 1.8% and 1.7% of the unit cell volume, values which are in agreement with those of **1** in the high-temperature phase (ca. 1.8%). This molecule lies on a 3-fold axis and a 2-fold axis simultaneously. The 2-fold axis goes through the nitrogen atom, perpendicular to the molecule, generating the second carbon atom, while the 3-fold axis goes through the carbon atoms of the molecule along the *c* crystallographic direction, giving rise to three different positions for the nitrogen atom, indicating that the dimethylammonium is disordered in three different positions. The isomorphous compound $[NH_2(CH_3)_2]_n[Fe^{III}Fe^{II}(HCOO)_6]_n$ presents an structural phase transition at 155 K that produces, besides slight variations in the three-dimensional arrangement, the blocking of the dimethylammonium molecule in three different positions, tripling the unit cell. The X-ray crystallographic studies at different temperatures between 30 and 105 K have revealed that the structures of compounds **2** and **3** are the same as those previously reported at RT, and therefore, no structural phase transition is observed for either of these complexes.

The determination of the position of the hydrogen atoms was carried out combining X-ray synchrotron and powder neutron diffraction data, both collected at the same temperature (45 K) slightly above the magnetic phase transition (ca. 37 K). A summary of the most important features obtained from the multipattern refinement can be found in Table 1. From these refinements we can discard a nuclear phase transition involving the ordering of the hydrogen atoms. However, the size and direction of the thermal ellipsoids of the $[NH_2(CH_3)_2]_n$ counterions suggest that this molecule is weakly anchored within the cavities. A comparison of the hydrogen bond distances for compounds **2** and **3** and for those previously studied for compound **1** is highlighted in Table 1. The shortening of the hydrogen bond distances upon cooling should be the responsible for the structural phase transition previously described[4c] and for the dielectric relaxation behavior observed for compound **1**.[22] However, for compounds **2** and **3**, it seems that the reorientation motion of the $[NH_2(CH_3)_2]_n$ counterions in the cavities is enough to preclude the occurrence of a structural phase transition.

A recent work on other heterometallic formate structures with formulas $[NH_2(CH_3)_2]_n[Fe^{III}M^{II}(HCOO)_6]_n$, with $M^{II} = Zn^{II}$,

DOI: 10.1021/acs.inorgchem.6b01866
Inorg. Chem. XXXX, XXX, XXX−XXX

Table 1. Comparison of Selected Geometric Parameters at 175 K Using Single-Crystal Neutron Diffraction Data for 1[4c] and Multipattern Refinement at 45 K for 2 and 3 (see main text)[a]

	1	2	3
Fe^{III}: Fe(1)−O(2)	2.0046(11)	2.0143(11)	2.009(2)
M^{II}: M(2)−O(1)	2.1196(13)	2.0765(17)	2.156(3)
C(1)−O(1)	1.2326(17)	1.2395(19)	1.245(3)
C(1)−O(2)	1.2606(16)	1.261(2)	1.266(4)
N(1)−C(2)	1.499(10)	1.486(11)	1.60(19)
N(1)···O(1)	3.046(2)	3.029(5)	3.039(7)
H···O(1)	2.13(3)	2.17(6)	2.09(7)
N(1)−H	0.99(1)	0.86(6)	1.05(5)
N(1)−H···O(1)	152(1)	168(4)	149(5)

[a]Distances in Angstroms; angles in degrees.

Ni^{II}, and Cu^{II},[23] has shown that M^{II} and Fe^{III} ions are distributed over the metal sites with equal probability. The synthetic routes of these compounds are very similar to those of compounds **2** and **3**, with only the number of hours kept at high temperature (140 °C) in the solvothermal protocol and the slope of the cooling ramp being different. The results obtained from the neutron diffraction refinement for **2** and **3** give rise to a model in which the M^{II} site does not show a significant metal disorder [neutron coherent scattering length for Fe, Co, and Mn are 9.45, 2.49, and −3.73 fm, respectively].

Magnetic Studies. For the determination of the magnetic structure of **2** and **3** (without applied magnetic field) below the ordering temperature ($T_N \approx 32$ and 35 K for **2** and **3**, respectively), a series of neutron diffraction measurements at different temperatures above and below T_N was carried out by using the high-flux and medium-resolution D1B powder diffractometer. The high-flux neutron diffraction pattern collected in the paramagnetic phase (ca. 45 K) was used to refine the low-temperature instrumental parameters. The Rietveld refinement was carried out using the crystal structure model (with fixed coordinates and rescaled displacement parameters) derived from the multipattern refinement.

The increase of intensity on some Bragg reflections in the neutron diffraction pattern at 2 K suggests the occurrence of a long-range magnetic ordering (see Figure 4), which is in agreement with the previous magnetometry measurements.[4b] The observed magnetic contribution, on top of nuclear reflections, suggests that the magnetic reflections can be indexed with the propagation vector $\mathbf{k} = (0, 0, 0)$. The indexing of the observed magnetic reflections was done using the k-Search program included in the FullProf suite, confirming the occurrence of a propagation vector $\mathbf{k} = (0, 0, 0)$.[24]

The weak magnetic contribution observed on these materials, together with the high overlapping between nuclear and magnetic reflections, and the background produced by the high number of hydrogen atoms in these compounds, with a ratio of 0.61 hydrogen atoms per non-hydrogen atom, precludes an accurate magnetic structure refinement directly from these patterns. These difficulties can partially be circumvented by working with difference patterns. For that we must subtract the normalized nuclear intensity of the paramagnetic phase collected at 45 K from the ordered phase pattern (ca. 2 K). This difference pattern isolates the magnetic contribution, and therefore, a more accurate indexing of the magnetic reflections and magnetic structure determination can be undertaken (see Figure 5).

The representational analysis technique described by Bertaut has been used to determine the possible magnetic structures compatible with the *P*-31*c* space group and propagation vector $\mathbf{k} = (0, 0, 0)$ for **2** and **3** compounds.[15a] Six irreducible representations of the group G_k, (Γ_1–Γ_6) and the corresponding set of basis vectors for each irreducible representation were determined using the program BasIreps.[15b] The representational analysis provides the expression of the magnetic moment Fourier components as linear combinations of basis vectors of the irreducible representations (*irreps*) of the propagation vector group G_k. The basis vectors describe the possible arrangements of magnetic structures. From the six possible *irreps* provided by BasIreps, Γ_1–Γ_4 are real and one dimensional while Γ_5 and Γ_6 are complex and two dimensional. The magnetic representation Γ_M for each magnetic site [Wyckoff position 2*b* for Fe(1) and for 2*c* for $M^{II}(1)$] can be decomposed

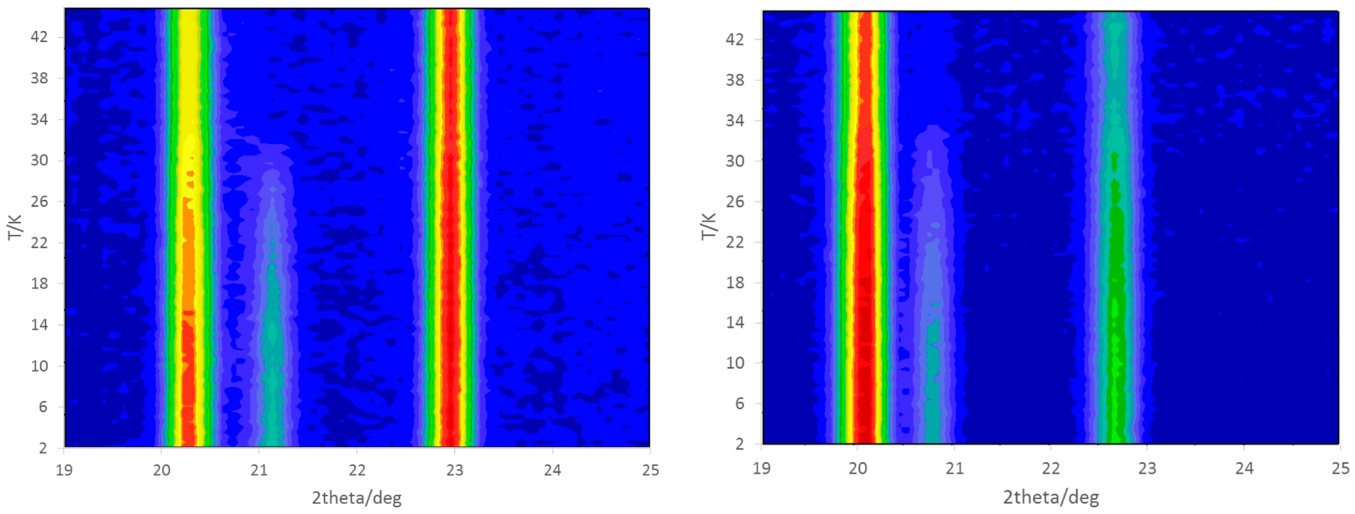

Figure 4. Detail of the mesh plot of the thermodiffractograms corresponding to compounds **2** (left) and **3** (right) collected at D1B in the temperature range of 2–45 K. It can be appreciated a clear increase of the reflections (1 0 0) (at a value of 2θ of 20.4° for **2** and 20.2° for **3**), (0 0 2) (at 2θ = 21.2° for **2** and 20.8° for **3**), and (1 0 1) (at 2θ = 23.0° for **2** and 22.7° for **3**).

DOI: 10.1021/acs.inorgchem.6b01866
Inorg. Chem. XXXX, XXX, XXX–XXX

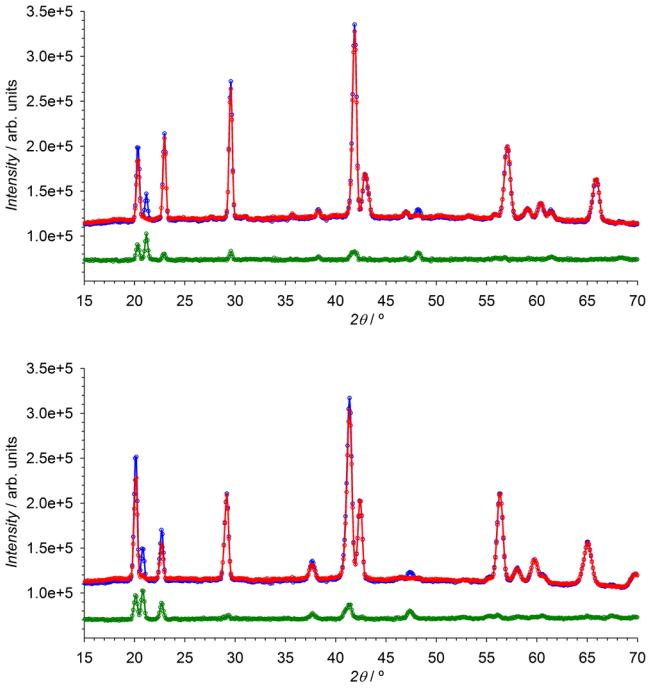

Figure 5. Neutron powder patterns of **2** (top) and **3** (bottom) collected at 1.5 (blue) and 45 K (red) using the high-flux D1B diffractometer. The difference diffraction pattern has been represented in green. The intensity of the calculated difference pattern has been shifted to an arbitrary value of ca. 58 000 units in order to achieve a similar background to those observed in the original patterns.

as a direct sum of *irreps* by applying the great orthogonality theorem. In the present case [where **k** = (0, 0, 0)], all Fourier coefficients must be real; therefore, the *irreps* from Γ_1−Γ_4 are in principle direct possible solutions. The complex 2D *irreps* should be converted to real, giving rise to a new set of possible magnetic structures. Since both metallic networks (M^{II} and Fe^{III}) become magnetically ordered at the same temperature, it is expected that the magnetic structure is described within the same magnetic representation. Γ_3 is the only 1D *irrep* that appears in the magnetic representation Γ_M for both Wyckoff positions (2*b* and 2*c*). However, this solution, where all magnetic moments are strictly along the *c* axis, is not able to reproduce the experimental data; then we have to analyze the 2D *irreps*.

An analysis of the complex representations shows that they can be transformed in two two-dimensional physically irreducible representations (PIR). We used BasIreps in the mode reading the PIR database provided in ref 15c. In the present case the Γ_5 and Γ_6 *irreps*, which are complex and two dimensional, can be transformed to real matrices (PIR: ${}^{P}\Gamma_6$ and ${}^{P}\Gamma_3$, respectively) by application of a unitary transformation (see Table 2).

The magnetic representation Γ_M for 2*b* and 2*c* Wyckoff positions (Fe^{III} and M^{II}, respectively) can be decomposed as a direct sum of PIR

$$\Gamma_M(2b) = {}^{P}\Gamma_1 \oplus {}^{P}\Gamma_2 \oplus {}^{P}\Gamma_3$$

$$\Gamma_M(2c) = {}^{P}\Gamma_2 \oplus {}^{P}\Gamma_3 \oplus {}^{P}\Gamma_5 \oplus {}^{P}\Gamma_6$$

Considering that both sublattices should be ordered within the same magnetic representation, the possible PIR are those that appear simultaneously in the decomposition of the magnetic representation of 2*b* and 2*c* sites. Then the magnetic structure

Table 2. Physically Irreducible Representations of the Space Group *P*-31c for k = (0, 0, 0)[a]

	(1|000)	$(3^{+}_{001}\|000)$	$(3^{-}_{001}\|000)$	$(2_{2x\bar{x}0}\|00\frac{1}{2})$	$(2_{x2\bar{x}0}\|00\frac{1}{2})$	$(2_{x\bar{x}00}\|00\frac{1}{2})$	(−1|000)	$(-3^{+}_{001}\|000)$	$(-3^{-}_{001}\|000)$	$(m_{0yz}\|00\frac{1}{2})$	$(m_{x0z}\|00\frac{1}{2})$	$(m_{xxz}\|00\frac{1}{2})$
${}^{P}\Gamma_1$	1	1	1	1	1	1	1	1	1	1	1	1
${}^{P}\Gamma_2$	1	1	1	−1	−1	−1	1	1	1	−1	−1	−1
${}^{P}\Gamma_3$	$\begin{pmatrix} 1 & 0 \\ 0 & 1 \end{pmatrix}$	$\begin{pmatrix} -a & -b \\ b & -a \end{pmatrix}$	$\begin{pmatrix} -a & b \\ -b & -a \end{pmatrix}$	$\begin{pmatrix} -a & -b \\ -b & a \end{pmatrix}$	$\begin{pmatrix} 1 & 0 \\ 0 & -1 \end{pmatrix}$	$\begin{pmatrix} -a & b \\ b & a \end{pmatrix}$	$\begin{pmatrix} 1 & 0 \\ 0 & 1 \end{pmatrix}$	$\begin{pmatrix} -a & -b \\ b & -a \end{pmatrix}$	$\begin{pmatrix} -a & b \\ -b & -a \end{pmatrix}$	$\begin{pmatrix} -a & -b \\ -b & a \end{pmatrix}$	$\begin{pmatrix} 1 & 0 \\ 0 & -1 \end{pmatrix}$	$\begin{pmatrix} -a & b \\ b & a \end{pmatrix}$
${}^{P}\Gamma_4$	1	1	1	1	1	1	−1	−1	−1	−1	−1	−1
${}^{P}\Gamma_5$	1	1	1	−1	−1	−1	−1	−1	−1	1	1	1
${}^{P}\Gamma_6$	$\begin{pmatrix} 1 & 0 \\ 0 & 1 \end{pmatrix}$	$\begin{pmatrix} -a & -b \\ b & -a \end{pmatrix}$	$\begin{pmatrix} -a & b \\ -b & -a \end{pmatrix}$	$\begin{pmatrix} -a & -b \\ -b & a \end{pmatrix}$	$\begin{pmatrix} 1 & 0 \\ 0 & -1 \end{pmatrix}$	$\begin{pmatrix} -a & b \\ b & a \end{pmatrix}$	$\begin{pmatrix} -1 & 0 \\ 0 & -1 \end{pmatrix}$	$\begin{pmatrix} a & b \\ -b & a \end{pmatrix}$	$\begin{pmatrix} a & -b \\ b & a \end{pmatrix}$	$\begin{pmatrix} a & b \\ b & -a \end{pmatrix}$	$\begin{pmatrix} -1 & 0 \\ 0 & 1 \end{pmatrix}$	$\begin{pmatrix} a & -b \\ -b & -a \end{pmatrix}$

[a]The symmetry elements are written according to Seitz's notation. $a = 1/2$ and $b = \sqrt{3}/2$. Notice that the ordering of PIR (database: PIR_data.txt, by Harold T. Stokes and Branton J. Campbell, 2013) is different than those obtained directly from the *irreps* calculations done by BasIreps.[15b] The magnetic space groups of the 1D *irreps* (all of them maximal subgroups of *P*-31c(1′)) are unambiguously determined as ${}^{P}\Gamma_1$: *P*-31c, ${}^{P}\Gamma_2$: *P*-31c′; ${}^{P}\Gamma_4$: *P*-3′1c′; ${}^{P}\Gamma_5$: *P*-3′1c. For the 2D *irreps* the magnetic space groups are of lower symmetry and depend on the particular basis vectors used to describe the magnetic structure.

DOI: 10.1021/acs.inorgchem.6b01866
Inorg. Chem. XXXX, XXX, XXX−XXX

Table 3. Basis Vectors of the Physically Irreducible Representations for the 2*b* and 2*c* Sites Which Give the Best Model for the Magnetic Structure[a]

					$^{2}BV_1$		
$^{P}\Gamma_2(GM_2^+)$	2*b* (0,0,0)	Fe^{III}	*x*, *y*, *z*		(0,0,1)		
			x, *x* − *y*, −*z* + 1/2		(0,0,1)		
	2*c* (1/3,2/3,1/4)	M^{II}	*x*, *y*, *z*		(0,0,1)		
			−*x*, −*y*, −*z*		(0,0,1)		
				$^{3}BV_1$	$^{3}BV_2$	$^{3}BV_3$	$^{3}BV_4$
$^{P}\Gamma_3(GM_3^+)$	2*b* (0,0,0)	Fe^{III}	*x*, *y*, *z*	(1,0,0)	(0,1,0)	(1, 2,0)	(−2, −1,0)
			x, *x* − *y*, −*z* + 1/2	(−1,0,0)	(1,1,0)	(−1, −2, 0)	(−1, 1, 0)
	2*c* (1/3,2/3,1/4)	M^{II}	*x*, *y*, *z*	(1,2,0)	(1,0,0)		
			−*x*, −*y*, −*z*	(1,2,0)	(1,0,0)		

[a]We added the notation of the *irreps* provided in the Bilbao Crystallographic Server.[25]

can only be described by $^{P}\Gamma_2$, $^{P}\Gamma_3$ or a combination of both PIR. In the case of the 2D *irrep* $^{P}\Gamma_3$ the associated magnetic structures are constrained to be in the *ab* plane, while the 1D *irrep* $^{P}\Gamma_2$ gives a contribution strictly along the *c* axis. The model described by $^{P}\Gamma_2$ is not able to fit the experimental data, while the models associated with $^{P}\Gamma_3$ give reasonably good agreement with experimental data. We explored the possible solutions without taking into account the symmetry using the simulated annealing procedure implemented in FullProf,[14] and this gives always a small component along the *c* axis. In order to account for this component, a combination of both PIR is necessary, Table 3.

We also used the program k-subgroupMag from the Bilbao Crystallographic Server[26] in order to determine the Shubnikov groups associated with the mixture of the two *irreps* $^{P}\Gamma_2$ and $^{P}\Gamma_3$. The only possible magnetic groups are *P*-1 and *C*2′/*c*′. The use of basis vectors $^{3}BV_1(Fe^{III})$, $^{3}BV_2(Fe^{III})$, $^{3}BV_1(M^{II})$, $^{2}BV_1(Fe^{III})$, and $^{2}BV_1(M^{II})$ give rise to the *P*-1 magnetic space group (see Figure S2). Using only five parameters we obtain a configuration (similar to that provided by *C*2′/*c*′ but with the moments rotated 30° around the *c* axis) that gives good results; however, the convergence of the refinement is not achieved when all parameters of *P*-1 (six free parameters) are included. The use of basis vectors $^{3}BV_3(Fe^{III})$, $^{3}BV_4(Fe^{III})$, $^{3}BV_2(M^{II})$, $^{2}BV_1(Fe^{III})$, and $^{2}BV_1(M^{II})$ gives rise to a configuration of 5 free parameters corresponding to one of the three equivalent variants of the *C*2′/*c*′ Shubnikov group (subgroups of *P*-31*c*1′). The occurrence of the three variants of *C*2′/*c*′ is due to the loss of the ternary axis at the magnetic transition in the parent group *P*-31*c*1′. The three possible orientations, with respect to the unit cell of the parent group, of the magnetic structure described by the *C*2′/*c*′ are shown in Figure S3. These models correspond to three different domains within a single crystal, so that in neutron powder diffraction the three variants contribute as different crystallites to the pattern.

The magnetic model described by the *C*2′/*c*′ Shubnikov group gives rise to a magnetic structure where the magnetic moments of both sites are mainly antiferromagnetically coupled in the *ab* plane with a small component along the *c* axis. As a result of peak overlap in the trigonal crystal system, neutron powder diffraction is not able to distinguish the absolute direction of the magnetic moments within the *ab* plane. On the basis of the ab initio calculations for compound **2**, the projection of the easy axis for the cobalt ions within the *ab* plane gives a value of 60° from the *a* direction (Variant 1). Moreover, according to the symmetry relations, the two symmetry-related Fe^{III} ions are not strictly antiferromagnetically coupled with the M^{II} ions. The Fe^{III} ions are slightly tilted among them, with angles of ca. 20° and 13° between adjacent Fe^{III} ions along the *c* axis for compounds **2** and **3**, respectively. The Rietveld refinement of the difference pattern using the mentioned combination of PIR is shown in Figure 6.

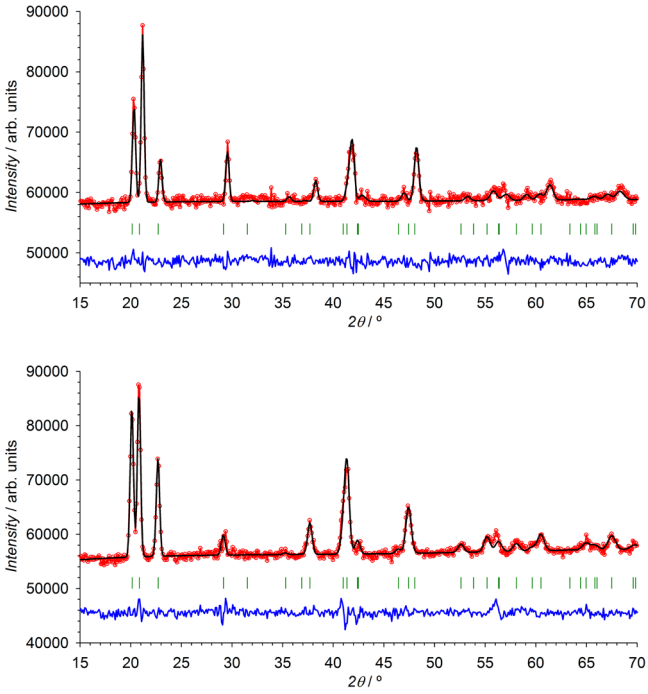

Figure 6. Fit of the difference pattern of compound **2** (top) and **3** (bottom) using the combination of both *p-irreps* ($^{P}\Gamma_2 \oplus {}^{P}\Gamma_3$) (see main text). Rietveld data refinement gives the agreement factors χ^2 = 3.87 and magnetic R_B = 12.9% for **2** and χ^2 = 3.22 and R_B = 7.26% for **3**. Experimental data have been represented as open red circles, calculated Rietveld patterns are shown as solid black lines, and differences between observed and calculated patterns have been plotted as solid blue lines. Vertical green marks represent the positions of the Bragg reflections.

Keeping in mind the crystal structure of **2** and **3**, let us describe their magnetic structures and compare them with that previously reported for **1**. The Fe^{III}(2*b*) and M^{II}(2*c*) atoms are connected between them through anti−anti carboxylate bridges. The Fe^{III}−M^{II} interaction through this bridge has an antiferromagnetic nature, as observed in magnetometry measurements. The antiferromagnetic coupling takes place mainly in the *ab* plane (see Figure 7, left). Each carboxylate group connects two ions with different valence along the [2/3, 1/3,

DOI: 10.1021/acs.inorgchem.6b01866
Inorg. Chem. XXXX, XXX, XXX−XXX

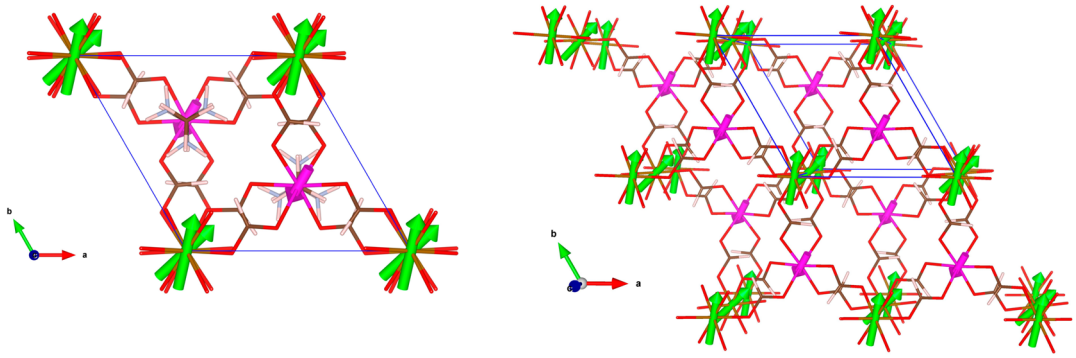

Figure 7. (Left) View along the *c* axis of the unit cell of compound **2**, together with the magnetic moment of the Co^{II} and Fe^{III} ions represented as pink and green arrows, respectively. (Right) Perspective view of a fragment of **2**, where the *ABAB* stacking sequence of the Fe^{III} ions along the *c* axis is noticed. A single unit cell has been represented together with the magnetic structure as reference for the reader. For the sake of clarity, the $[NH_2(CH_3)_2]^+$ counterions have been omitted in this figure. The modulus of each arrow has been proportionally scaled to the magnetic moment of each magnetic site.

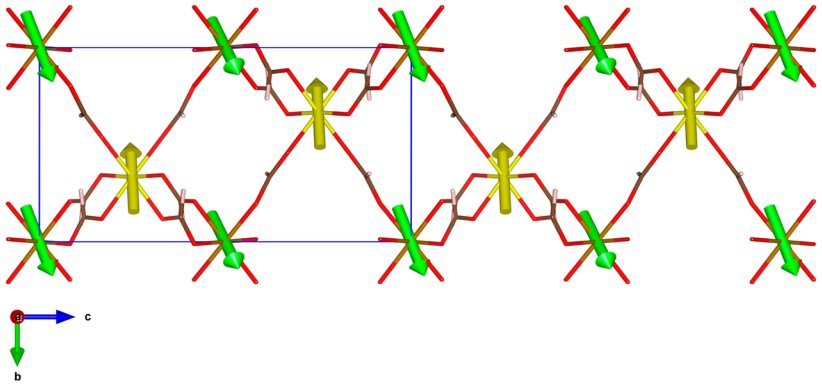

Figure 8. View along the *a* axis of the unit cell of compound **3**, together with the magnetic moments of the Mn^{II} and Fe^{III} ions represented as yellow and green arrows, respectively. Occurrence of a weak canting along the *c* axis is clearly observed. For the sake of clarity, only the $[Fe^{III}Mn^{II}(HCOO)_6]_n$ framework has been represented, together with the magnetic structure obtained from Rietveld refinement. The modulus of each arrow has been proportionally scaled to the magnetic moment of each magnetic site.

−1/4], [−1/3, −2/3, −1/4], [−1/3, 1/3, −1/4], [−2/3, −1/3, 1/4], [1/3, 2/3, 1/4], and [1/3, −1/3, 1/4] directions, giving rise to the final three-dimensional structure. It deserves to be noted that according to the crystal structure, all carboxylate groups are symmetry related and therefore equivalent. However, from a magnetic point of view the exchange coupling of these carboxylate groups should be slightly different, giving rise to the two different magnetic orientations of the Fe^{III} ions. This ultimately means that the magnetic space group has lower symmetry than the paramagnetic group. We cannot refine the crystal structure in the monoclinic group because within our precision we do not see significant variation of the nuclear intensities.

The macroscopic magnetic measurements of **2** show the occurrence of an antiferromagnetic coupling between the neighboring metal ions. Nevertheless, below T_N the susceptibility exhibits a sharp increase. This feature is compatible with a ferrimagnetic behavior probably due to the noncompensation of the magnetic moments of the different ions present in this compound. From the neutron diffraction experiments, this scenario is confirmed; the refined magnetic moments of the $Fe^{III}(2b)$ and the $Co^{II}(2c)$ atoms are 4.33(9) and 2.5(1) μ_B, respectively. The modulus of the resultant magnetization calculated for a molecular unit $\mathbf{M} = \{[\mathbf{m}_{2b}(I) + \mathbf{m}_{2b}(II) + \mathbf{m}_{2c}(I) + \mathbf{m}_{2c}(III)]/2\}$ [with (I) = *x*, *y*, *z*; (II) = −*y*, −*x*, −*z* + 1/2; (III) = −*x*, −*y*, −*z*] is approximately 1.7 μ_B, which is slightly low for a collinear ferrimagnet with opposite spins *S*= 5/2 and 3/2 (2 μ_B). However, a small deviation of the value of 2 μ_B for completely polarized magnetic spins and antiferromagnetic coupling is possible when the magnetic moments are not strictly collinear or when a spin delocalization effect occurs. Therefore, this model produces a ferrimagnetic layered structure, where the layers formed by the magnetic moments of the Co^{II} ions follow an *AAA* sequence, while the layers formed for the Fe^{III} ions follows an *ABAB* sequence, both packed along the *c* axis (see Figure 7, right). Along the *c* axis, the magnetic contribution on the Co(II) site is notably weaker than the component on the Fe^{III} site. Moreover, the refined structure gives rise to a model where both sites are antiferromagnetically coupled along the *c* axis.

The magnetic measurements of **3** are slightly different from those of **1** or **2**, since both metallic centers have the same spin state, with *S* = 5/2. The electronic configurations of the high-spin Mn^{II} and Fe^{III} are also very similar, both being spin sextets with A_{1g} as the orbital ground state in the case of O_h symmetry and with Landé factors close to 2.0. Therefore, we expect a collinear antiferromagnetic coupling between both ions. The magnetometry measurements show a global antiferromagnetic behavior, which was corroborated by the negative value of the Weiss constant after the Curie−Weiss fit of the experimental data. However, at T_N the susceptibility curve as a function of the temperature presents a jump, which should be due either to

DOI: 10.1021/acs.inorgchem.6b01866
Inorg. Chem. XXXX, XXX, XXX−XXX

the noncompensation of the magnetic moments of both networks or to the occurrence of a weak spin canting. The refined magnetic moments for each magnetic site give a similar value, being slightly lower for Fe^{III} than for Mn^{II} ion [4.3(1) and 4.4(1) μ_B, respectively]. This feature, together with the packing sequence of the Fe^{III} ions, which follow the same order as in compound **2**, produces a noncompensation of the magnetic moment within the *ab* plane. Moreover, the fit of the data gives a component of the magnetic moments along the *c* axis for the Fe^{III} sites, which produces a tilting of the magnetic moment with respect to the *ab* plane of around 15(5)° (see Figure 8). This tilting angle has the same sign for all Fe^{III} sites. However, the refined value of the magnetic contribution along the *c* axis of the Mn^{II} ion is zero within the experimental error. Therefore, this model is compatible with the occurrence of a spin canting. The magnetic moments obtained after the Rietveld refinement using the combination of ${}^{P}\Gamma_2$ and ${}^{P}\Gamma_3$ are listed in Table 4.

Table 4. Magnetic Moment Components Determined for Each Atom Site through Rietveld Refinement Using the Combination of ${}^{P}\Gamma_2$ and ${}^{P}\Gamma_3$ (Shubnikov group $C2'/c'$) and Calculated Magnetic Moments Obtained from DFT Studies for Compounds 2 and 3[a]

2	M_a	M_b	M_c	M_{total}	M_{DFT}
Fe(1)	3.2(3)	4.6(2)	1.5(6)	4.33(8)	4.367
Co(1)	−2.2(3)	−2.2(3)	−1.0(7)	2.44(10)	2.801
3	M_a	M_b	M_c	M_{total}	M_{DFT}
Fe(1)	3.5(3)	4.4(3)	1.5(5)	4.32(10)	4.364
Mn(1)	−4.44(11)	−4.44(11)	−0.2(5)	4.44(10)	4.688

[a]Atomic positions: Fe^{III} = (0, 0, 0) and M^{II} = (1/3, 2/3, 1/4)

The modulus of the resultant magnetization calculated for formula M = $\{[\mathbf{m}_{2b}(I) + \mathbf{m}_{2b}(II) + \mathbf{m}_{2c}(I) + \mathbf{m}_{2c}(III)]/2\}$ [with (I) = *x*, *y*, *z*; (II) = −*y*, −*x*, −*z* + 1/2; (III) = −*x*, −*y*, −*z*] is approximately 1.4 μ_B. The projections in the *ab* plane of the magnetic moments of Fe^{III} and Mn^{II} are ca. 3.97(30) μ_B and 4.44(11) μ_B. The difference between them is 0.5 μ_B, a value which is smaller than the component along the *c* axis. Consequently, it is reasonable to think that the signal observed in the magnetometry measurements should be mainly produced by the occurrence of a canting along the *c* axis. The refined magnetic structures for **2** and **3** are therefore compatible with the macroscopic magnetic measurements; moreover, the refined values of the magnetic moments are in good agreement with other metal−organic compounds.[27] However, the values of the magnetic moments obtained for the Fe^{III} sites are slightly higher than those previously observed for compound **1**, suggesting that the possible delocalization of the magnetic moment into the bridging ligands is less important.

Before finishing this section, we would like to compare the obtained magnetic structures for compounds **2** and **3** with those previously reported for **1**. All compounds present layered antiferromagnetic structures stacked along the *c* axis. The most remarkable feature is the orientation of the magnetic moments of **1** compared with those obtained for **2** and **3**. In compounds **2** and **3**, the magnetic moments are contained mainly within the *ab* plane, with a small canting angle along the *c* axis, in particular for compound **3**. In contrast, in compound **1** the magnetic moments are mainly along the *c* axis. The magnetic moment of Fe^{III} is symmetry constrained to be along the *c* axis, and the main contribution of the Fe^{II} ion is along the *c* axis with a small component in the *ab* plane. This feature is compatible with our DFT calculations, which prove that the anisotropic easy axis of the Fe^{II} is along the *c* axis and therefore induces an antiferromagnetic coupling along the *c* axis. Compound **1** presents a tripling of the *c* axis due to the occurrence of a structural phase transition giving rise to a variation in the staking sequence of the magnetic moments compared to those obtained for **2** and **3**. The in-plane component of the magnetic moments in compound **2** is highly influenced by the occurrence of an easy axis contained in the *ab* plane, the DFT calculations having proved that the anisotropic easy axis for the Co^{II} ion is mainly contained in the *ab* plane and along the [1 1 0] crystallographic direction. For compound **3**, the DFT calculations show an almost isotropic system, which is reasonable for Mn^{II} ions. In that case, the in-plane conformation of the magnetic moments should be related with the competition between the single-ion anisotropy and the dipolar energy, both of similar magnitude for Mn^{II}. A similar effect has been reported on the $Mn(COOH)_2{\cdot}2H_2O$ compound, where the magnetic moment does not follow the easy direction obtained from the dipolar energy calculations.[28]

Moreover, compound **1** is the only one presenting a negative magnetization under small external field. In the case of compound **3**, this effect is not expected due to both metal sites (Mn^{II} and Fe^{III}) having very similar electronic configuration. However, in the case of compound **2**, where the difference in the electronic configuration is notable, a negative magnetization effect could be expected. However, the absence of this negative magnetization in the cobalt compound can be explained taking into account that both metallic networks become ordered at the same time, and therefore, there is no "inductive effect" from one network over the other. A similar negative magnetization has been previously reported for oxalate bimetallic (Fe^{II} and the Fe^{III} ions) compounds.[29] The main difference in these compounds compared with **1** is that the Fe^{II} and the Fe^{III} ions are contained in the same *ab* plane and separated by an organic molecule. The separation between $[Fe^{II}Fe^{III}(ox)_3]$ (ox = oxalate) layers can be tuned by changing the spacer organic molecule, and surprisingly, the order temperature increases with the increase of the distance between layers. From neutron diffraction experiments,[30] a magnetic model has been proposed, the magnetic moments of both metallic centers lying along the *c* axis with an antiferromagnetic coupling between Fe^{II} and Fe^{III} within the layers. The overall magnetic structure is similar to that observed for compound **1**. Similarly to our case, the substitution of Fe^{II} for another divalent transition metal produces the vanishing of the negative magnetization effect,[31] as has been also observed in compounds **2** and **3**. In a recent work presented by Ciupa et al.[22] the authors present a compound of formula $[NH_2(CH_3)_2]_n[Fe^{III}Mg^{II}(HCOO)_6]_n$ which crystallizes in the same space group as compounds **2** and **3**, even at low temperature, and presents a negative magnetization. Although the authors do not report magnetization curves as a function of different crystal orientations, which would be useful to propose a possible magnetic structure model, the partial substitution of Mg^{II} by Fe^{II} suggests a magnetic structure similar to **1**. The influence in the magnetic behavior of the counterion in the iron-based niccolite compounds has also been recently investigated.[32] The inclusion of ethylammonium or diethylammonium cations within the niccolite framework gives rise to isostructural compounds with similar magnetic behavior to that described for compound **1**. However, the resultant component of the magnetic moment is

DOI: 10.1021/acs.inorgchem.6b01866
Inorg. Chem. XXXX, XXX, XXX−XXX

slightly lower than that expected for noncompensated networks of Fe(III) and Fe(II), suggesting that the magnetic moments in these compounds are not strictly antiparallel. Further studies in these compounds are needed in order to understand the mechanism that promotes the occurrence of negative magnetization.

In summary, the above results confirm the occurrence of a long-range magnetic order formed by two different networks corresponding to the Fe^{III} and M^{II} metal ions. The noncompensation of the magnetic moment of the different magnetic ions present in the crystal is responsible for the ferrimagnetic behavior in compounds **1** and **2**, while in **3** the ferromagnetic signal arises from a weak spin canting along the *c* axis.

CONCLUSIONS

In this work we have refined the crystal structure of $[NH_2(CH_3)_2]_n[Fe^{III}M^{II}(HCOO)_6]_n$, with M^{II} = Co^{II} (**2**) and Mn^{II} (**3**) ions, by combining high-resolution neutron diffraction together with synchrotron X-ray diffraction at 45 K. This multipattern refinement permits the localization of the hydrogen atoms of the $[NH_2(CH_3)_2]^+$ counterions and discards the occurrence of a structural phase transition. The refined structural models have been used as the starting point for the refinement of the magnetic structures. On the basis of the symmetry analysis, we obtained two possible physically irreducible representations (*p-irreps*) that have been combined (magnetic space group $C2'/c'$) to explain the experimental data. The magnetic structure of **2** consists in a noncompensated antiferromagnetic arrangement where the magnetic moments are contained in the *ab* plane. In contrast, for compound **3** the magnetic structure is almost antiferromagnetic within the *ab* plane with a spin canting along the *c* axis. The magnetic structures have been correlated with DFT calculations, which give us the direction of the easy axis and an estimation of the magnetic moment residing on the magnetic sites.

ASSOCIATED CONTENT

Supporting Information

The Supporting Information is available free of charge on the ACS Publications website at DOI: 10.1021/acs.inorgchem.6b01866.

Structure determination and refinement details, X-ray crystallographic data in CIF format, magnetic cif files for $C2'/c'$ Shubnikov group using variant 1, selected geometric parameters as a function of the temperature for compounds **2** and **3**, multipattern refinement of compound **3** collected at 45.0 K, scheme of the $P\bar{1}$ Shubnikov group and the three possible magnetic variants for $C2'/c'$ magnetic space group (PDF)
(ZIP)
(ZIP)

AUTHOR INFORMATION

Corresponding Authors

*E-mail: fabelo@ill.fr.
*E-mail: jrc@ill.fr.
*E-mail: buxh@nankai.edu.cn.

ORCID

Oscar Fabelo: 0000-0001-6452-8830

Notes

The authors declare no competing financial interest.

ACKNOWLEDGMENTS

The authors are grateful to ILL instruments for the neutron beam-time allocated (doi:10.5291/ILL-DATA.5-31-2263). We also acknowledge SOLEIL for provision of synchrotron radiation facilities, and we would like to thank Dr. Pierre Fertey for assistance in using beamline CRISTAL. Partial funding for this work is provided by the Ministerio Español de Ciencia e Innovación through projects MAT2011-27233-C02-02 and MAT2011-25991 and Centro Universitario de la Defensa de Zaragoza through CUD 2013-17. J.A.R.V. acknowledges CSIC for a JAEdoc contract.

REFERENCES

(1) See for example: (a) Coronado, E.; Palacio, F.; Veciana, J. Molecule-Based Magnetic Materials. *Angew. Chem., Int. Ed.* **2003**, *42*, 2570−2572. (b) Kahn, O. *Molecular Magnetism*; Wiley-VCH: Weinheim, 1993. (c) Coronado, E.; Day, P. Magnetic Molecular Conductors. *Chem. Rev.* **2004**, *104*, 5419−5448. (d) Evangelisti, M.; Luis, F.; de Jongh, L. J.; Affronte, M. Magnetotherma properties of molecule-based materials. *J. Mater. Chem.* **2006**, *16*, 2534−2549. (e) Thomas, L.; Lionti, F.; Ballou, P.; Gatteschi, D.; Sessoli, R.; Barbara, B. Macroscopic Quantum Tunnelling of Magnetization in a Single Crystal of Nanomagnets. *Nature* **1996**, *383*, 145−147. (f) Ruiz, E.; Alemany, P.; Alvarez, S.; Cano, J. Structural Modeling and Magneto−Structural Correlations for Hydroxo-Bridged Copper(II) Binuclear Complexes. *Inorg. Chem.* **1997**, *36*, 3683−3688. (g) Wang, S.; Zuo, J.-L.; Gao, S.; Song, Y.; Zhou, H.-C.; Zhang, Y.-Z.; You, X.-Z. The Observation of Superparamagnetic Behavior in Molecular Nanowires. *J. Am. Chem. Soc.* **2004**, *126*, 8900−8901. (h) Berg, N.; Rajeshkumar, T.; Taylor, S. M.; Brechin, E. K.; Rajaraman, G.; Jones, L. F. What Controls the Magnetic Interaction in Bis-μ-alkoxo Mn III Dimers? A Combined Experimental and Theoretical Exploration. *Chem. - Eur. J.* **2012**, *18*, 5906−5918. (i) Cucinotta, G.; Perfetti, M.; Luzon, J.; Etienne, M.; Car, P. E.; Caneschi, A.; Calvez, G.; Bernot, K.; Sessoli, R. Magnetic Anisotropy in a Dysprosium/DOTA Single-Molecule Magnet: Beyond Simple Magneto-Structural Correlations. *Angew. Chem., Int. Ed.* **2012**, *51*, 1606−1610. (j) Adhikary, A.; Sheikh, J. A.; Konar, A. D.; Konar, S. Synthesis, Crystal Structure, Magnetic Study and Magneto-Structural Correlation of Three Cu (II) Complexes Formed via Pyridine bis (hydrazone) Based Ligand. *RSC Adv.* **2014**, *4*, 12408−12414.

(2) See, for example: (a) Xu, H.-B.; Wang, B. W.; Pan, F.; Wang, Z. M.; Gao, S. Stringing Oxo-Centered Trinuclear [MnIII3O] Units into Single-Chain Magnets with Formate or Azide Linkers. *Angew. Chem., Int. Ed.* **2007**, *46*, 7388−7392. (b) Zhao, J.-P.; Han, S.-D.; Zhao, R.; Yang, Q.; Chang, Z.; Bu, X.-H. Tuning the Structure and Magnetism of Heterometallic Sodium (1+)−Cobalt (2+) Formate Coordination Polymers by Varying the Metal Ratio and Solvents. *Inorg. Chem.* **2013**, *52*, 2862−2869. (c) Stroppa, A.; Barone, P.; Jain, P.; Pérez-Mato, J. M.; Picozzi, S. Hybrid Improper Ferroelectricity in a Multiferroic and Magnetoelectric Metal-Organic Framework. *Adv. Mater.* **2013**, *25*, 2284−2290. (d) Tian, Y.; Stroppa, A.; Chai, Y.; Yan, L.; Wang, S.; Barone, P.; Picozzi, S.; Sun, Y. Cross Coupling Between Electric and Magnetic Orders in a Multiferroic Metal-Organic Framework. *Sci. Rep.* **2014**, *4*, 6062.

(3) Cadiou, C.; Coxall, R. A.; Graham, A.; Harrison, A.; Helliwell, M.; Parsons, S.; Winpenny, R. E. P. Octanuclear Cobalt and Nickel Cages Featuring Formate Ligands. *Chem. Commun.* **2002**, 1106−1107.

(4) (a) Hagen, K. S.; Naik, S. G.; Huynh, B. H.; Masello, A.; Christou, G. Intensely Colored Mixed-Valence Iron (II) Iron (III) Formate Analogue of Prussian Blue Exhibits Néel N-type Ferrimagnetism. *J. Am. Chem. Soc.* **2009**, *131*, 7516−7517. (b) Zhao, J.-P.; Hu, B.-W.; Lloret, F.; Tao, J.; Yang, Q.; Zhang, X.-F.; Bu, X.-H. Magnetic Behavior Control in Niccolite Structural Metal Formate Frameworks [NH2(CH3)2][FeIIIMII(HCOO)6](M= Fe, Mn, and Co) by Varying the Divalent Metal Ions. *Inorg. Chem.* **2010**, *49* (22), 10390−10399. (c) Cañadillas-Delgado, L.; Fabelo, O.; Rodríguez-

DOI: 10.1021/acs.inorgchem.6b01866
Inorg. Chem. XXXX, XXX, XXX−XXX

Velamazan, J. A.; Lemee-Cailleau, M.-H.; Mason, S. A.; Pardo, E.; Lloret, F.; Zhao, J.-P.; Bu, X.-H.; Simonet, V.; Colin, C. V.; Rodríguez-Carvajal, J. The Role of Order−Disorder Transitions in the Quest for Molecular Multiferroics: Structural and Magnetic Neutron Studies of a Mixed Valence Iron(II)−Iron(III) Formate Framework. *J. Am. Chem. Soc.* **2012**, *134*, 19772−19781. (d) Chen, S.; Shang, R.; Hu, K.-L.; Wang, Z.-M.; Gao, S. [NH2NH3][M(HCOO)3] (M = Mn2+, Zn2+, Co2+ and Mg2+): Structural Phase Transitions, Prominent Dielectric Anomalies and Negative Thermal Expansion, and Magnetic Ordering. *Inorg. Chem. Front.* **2014**, *1*, 83−98. (e) Greenfield, J. T.; Kamali, S.; Izquierdo, N.; Chen, M.; Kovnir, K. NH4FeCl2 (HCOO): Synthesis, Structure, and Magnetism of a Novel Low-Dimensional Magnetic Material. *Inorg. Chem.* **2014**, *53* (6), 3162−3169. (f) Shang, R.; Chen, S.; Wang, B.-W.; Wang, Z.-M.; Gao, S. Temperature-Induced Irreversible Phase Transition From Perovskite to Diamond But Pressure-Driven Back-Transition in an Ammonium Copper Formate. *Angew. Chem., Int. Ed.* **2016**, *55*, 2097−2100. (g) Zhao, J.-P.; Han, S.-D.; Jiang, X.; Liu, S.-J.; Zhao, R.; Chang, Z.; Bu, X-H A Heterometallic Strategy to Achieve a Large Magnetocaloric Effect in Polymeric 3d Complexes. *Chem. Commun.* **2015**, *51*, 8288−8291.

(5) (a) Rodríguez-Velamazán, J. A.; Fabelo, O.; Beavers, C. M.; Natividad, E.; Evangelisti, M.; Roubeau, O. A Multifunctional Magnetic Material under Pressure. *Chem. - Eur. J.* **2014**, *20* (26), 7956−7961. (b) Real, J. A.; Andrés, E.; Muñoz, M. C.; Julve, M.; Granier, T.; Bousseksou, A.; Varret, F. Spin Crossover in a Catenane. *Science* **1995**, *268* (5208), 265−267. (c) Ohkoshi, S.; Imoto, K.; Tsunobuchi, Y.; Takano, S.; Tokoro, H. Light-Induced Spin-Crossover Magnet. *Nat. Chem.* **2011**, *3*, 564−569.

(6) (a) Mabbs, F. E.; Machin, D. J. *Magnetism and Transition Metal Complexes*; Chapman and Hall: London, 1973. (b) Figgis, B. N.; Hitchman, M. A. *Ligand Field Theory and its Applications*; Wiley-VCH: New York, 2000. (c) Armentano, D.; de Munno, G.; Lloret, F.; Julve, M. Novel Three-Dimensional Cage Assembly of a μ4-Carbonato-Bridged Cobalt (II) Compound [Co2 (bpm)(H2O) 2 (CO3) (OH)] NO3· 4H2O. *Inorg. Chem.* **1999**, *38*, 3744−3747. (d) Lloret, F.; Julve, M.; Cano, J.; Ruiz-García, R.; Pardo, E. Magnetic Properties of Six-Coordinated High-Spin Cobalt (II) Complexes: Theoretical Background and Its Application. *Inorg. Chim. Acta* **2008**, *361*, 3432−3445. (e) Zhao, J.-P.; Yang, Q.; Liu, Z.-Y.; Zhao, R.; Hu, B.-W.; Du, M.; Chang, Z.; Bu, X-H A Unique Substituted Co(II)-Formate Coordination Framework Exhibits Weak Ferromagnetic Single-Chain-Magnet Like Behavior. *Chem. Commun.* **2012**, *48*, 6568−6570. (f) Aromi, G.; Brechin, E. K. *Synthesis of 3d metallic single-molecule magnets*; Springer-Verlag: Berlin Heidelberg, 2006.

(7) (a) Kieslich, G.; Sun, S.; Cheetham, A. K. Solid-State Principles Applied to Organic−Inorganic Perovskites: New Tricks for an Old Dog. *Chem. Sci.* **2014**, *5*, 4712−4715. (b) Shannon, R. D. Revised Effective Ionic Radii and Systematic Studies of Interatomic Distances in Halides and Chalcogenides. *Acta Crystallogr., Sect. A: Cryst. Phys., Diffr., Theor. Gen. Crystallogr.* **1976**, *32*, 751−767.

(8) *CrysAlis PRO*; Agilent Technologies UK Ltd.: Yarnton, England, 2011.

(9) Sheldrick, G. M. Crystal Structure Refinement with SHELXL. *Acta Crystallogr., Sect. C: Struct. Chem.* **2015**, *71*, 3−8.

(10) Nardelli, M. PARST95 - An Update to PARST: a System of Fortran Routines for Calculating Molecular Structure Parameters from the Results of Crystal Structure Analyses. *J. Appl. Crystallogr.* **1995**, *28*, 659−659.

(11) Spek, A. L. Single-Crystal Structure Validation with the Program PLATON. *J. Appl. Crystallogr.* **2003**, *36*, 7−13.

(12) Momma, K.; Izumi, F. VESTA 3 for three-dimensional visualization of crystal, volumetric and morphology data. *J. Appl. Crystallogr.* **2011**, *44*, 1272−1276.

(13) (a) Richard, D.; Ferrand, M.; Kearley, G. J. Analysis and Visualisation of Neutron-Scattering Data. *J. Neutron Res.* **1996**, *4*, 33−39. (b) LAMP, the Large Array Manipulation Program. http://www.ill.eu/data_treat/lamp/the-lamp-book/.

(14) Rodriguez-Carvajal, J. Recent Advances in Magnetic Structure Determination by Neutron Powder Diffraction *Phys. B*, **1993**, *192*, 55−69. The programs of the FullProf Suite can be obtained at http://www.ill.eu/sites/fullprof.10.1016/0921-4526(93)90108-I

(15) (a) Bertaut, E. F. *Magnetism*, Vol. *III*, Ch. 4, Rado, G. T., Shul, H., Eds.; Academic Press, New York, 1963;. (b) Rodriguez-Carvajal, J. *BasIreps program* ILL-August 2007;. (c) Stokes, H. T.; Campbell, B. J.; Cordes, R. Tabulation of Irreducible Representations of the Crystallographic Space Groups and Their Superspace Extensions. *Acta Crystallogr., Sect. A: Found. Crystallogr.* **2013**, *69*, 388−395.

(16) Hohenberg, P.; Kohn, W. Inhomogeneous Electron Gas. *Phys. Rev.* **1964**, *136*, B864.

(17) Perdew, J. P.; Burke, K.; Ernzerhof, M. Generalized Gradient Approximation Made Simple. *Phys. Rev. Lett.* **1996**, *77*, 3865.

(18) Blöchl, P. E.; Jepsen, O.; Andersen, O. K. Improved Tetrahedron Method for Brillouin-Zone Integrations. *Phys. Rev. B: Condens. Matter Mater. Phys.* **1994**, *49*, 16223.

(19) (a) Kresse, G.; Furthmüller, J. Efficient Iterative Schemes for *ab initio* Total-Energy Calculations using a Plane-Wave Basis Set. *Phys. Rev. B: Condens. Matter Mater. Phys.* **1996**, *54*, 11169. (b) Kresse, G.; Furthmüller, J. Efficiency of ab-initio Total Energy Calculations for Metals and Semiconductors using a Plane-Wave Basis Set. *Comput. Mater. Sci.* **1996**, *6*, 15−50.

(20) Anisimov, V. I.; Aryasetiawan, F.; Lichtenstein, A. I. First-principles Calculations of the Electronic Structure and Spectra of Strongly Correlated Systems: the LDA+ U Method. *J. Phys.: Condens. Matter* **1997**, *9*, 767.

(21) Dudarev, S. L.; Botton, G. A.; Savrasov, S. Y.; Humphreys, C. J.; Sutton, A. P. Electron-Energy-Loss Spectra and the Structural Stability of Nickel Oxide: An LSDA+U Study. *Phys. Rev. B: Condens. Matter Mater. Phys.* **1998**, *57*, 1505.

(22) (a) Ciupa, A.; Maczka, M.; Gagor, A.; Sieradzki, A.; Trzmiel, J.; Pikul, A.; Ptak, M. Temperature-Dependent Studies of [(CH3)-2NH2][FeIIIMII(HCOO)6] Frameworks (MII = Fe and Mg): Structural, Magnetic, Dielectric and Phonon Properties. *Dalton Trans* **2015**, *44*, 8846−8854. (b) Sieradzki, A.; Pawlus, S.; Tripathy, S. N.; Gagor, A.; Ciupa, A.; Maczka, M.; Paluch, M. Dielectric relaxation behavior in antiferroelectric metal organic framework [(CH3)2NH2]-[FeIIIFeII(HCOO)6] single crystals. *Phys. Chem. Chem. Phys.* **2016**, *18*, 8462−8467.

(23) Ciupa, A.; Maczka, M.; Gagor, A.; Pikul, A.; Ptak, M. Synthesis and Characterization of Novel Niccolites [(CH3)2NH2][FeIIIMII-(HCOO)6] (MII = Zn, Ni, Cu). *Dalton Trans* **2015**, *44*, 13234−13241.

(24) Rodríguez-Carvajal, J. *k-Search program*; ILL, Aug 2007.

(25) (a) Aroyo, M. I.; Perez-Mato, J. M.; Capillas, C.; Kroumova, E.; Ivantchev, S.; Madariaga, G.; Kirov, A.; Wondratschek, H. Bilbao Crystallographic Server I: Databases and crystallographic computing programs. *Z. Kristallogr. - Cryst. Mater.* **2006**, *221* (1), 15−27. (b) Aroyo, M. I.; Kirov, A.; Capillas, C.; Perez-Mato, J. M.; Wondratschek, H. Bilbao Crystallographic Server II: Representations of crystallographic point groups and space groups″. *Acta Crystallogr., Sect. A: Found. Crystallogr.* **2006**, *62*, 115−128.

(26) Aroyo, M. I.; Perez-Mato, J. M.; Orobengoa, D.; Tasci, E.; de la Flor, G.; Kirov, A. Crystallography Online: Bilbao Crystallographic Server. *Bulg. Chem. Commun.* **2011**, *43*, 183−197.

(27) (a) Mesbah, A.; Sibille, R.; Mazet, T.; Malaman, B.; Lebegue, S.; Francois, M. Magnetism in the (Co1−xFex)2(OH)2(C8H4O4) Solid Solutions: a Combined Neutron Diffraction and Magnetic Measurements Study. *J. Mater. Chem.* **2010**, *20*, 9386−9391. (b) Sibille, R.; Lhotel, E.; Mazet, T.; Malaman, B.; Ritter, C.; Ban, V.; François, M. Magnetic Structure and Dynamics of a Strongly One-Dimensional CobaltII Metal-Organic Framework. *Phys. Rev. B: Condens. Matter Mater. Phys.* **2014**, *89*, 104413. (c) Díaz-Gallifa, P.; Fabelo, O.; Pasán, J.; Cañadillas-Delgado, L.; Rodríguez-Carvajal, J.; Lloret, F.; Julve, M.; Ruiz-Pérez, C. Synthesis, Crystal Structure, and Magnetic Characterization of the Three-Dimensional Compound [Co2(cbut)(H2O)3]n (H4cbut = 1,2,3,4-Cyclobutanetetracarboxylic Acid). *Inorg. Chem.* **2014**, *53*, 5674−5683. (d) Fabelo, O.; Cañadillas-Delgado, L.; Pasán, J.; Díaz-Gallifa, P.; Ruiz-Pérez, C.; Lloret, F.; Julve, M.; Puente Orench, I.; Campo, J.; Rodríguez-Carvajal, J. Neutron Diffraction Studies of the

DOI: 10.1021/acs.inorgchem.6b01866
Inorg. Chem. XXXX, XXX, XXX−XXX

Molecular Compound [Co2(bta)]n (H4bta = 1,2,4,5-Benzenetetracarboxylic Acid): In the Quest of Canted Ferromagnetism. *Inorg. Chem.* **2013**, *52*, 12818−12827. (e) Sibille, R.; Mesbah, A.; Mazet, T.; Malaman, B.; Capelli, S.; François, M. Magnetic Measurements and Neutron Diffraction Study of the Layered Hybrid Compounds Mn(C8H4O4)(H2O)2 and Mn2(OH)2(C8H4O4). *J. Solid State Chem.* **2012**, *186*, 134−141.

(28) Burlet, P.; Rossat-Mignot, J.; De combarieu, A.; Bedin, E. Magnetic Behaviour of the Dihydrate Formates $M(HCOO)_2$ 2 H_2O of the Transition Metals M = Mn, Fe, Co, N. *Phys. Status Solidi B* **1975**, *71*, 675−685.

(29) (a) Mathonière, C.; Nuttall, C. J.; Carling, S. G.; Day, P. Ferrimagnetic Mixed-Valency and Mixed-Metal Tris(oxalato)iron(III) Compounds: Synthesis, Structure, and Magnetism. *Inorg. Chem.* **1996**, *35*, 1201−1206. (b) Clemente-León, M.; Coronado, E.; Gómez-García, C. J.; Soriano-Portillo, A. Increasing the Ordering Temperatures in Oxalate-Based 3D Chiral Magnets: the Series [Ir(ppy)2(bpy)][M(II)M(III) (ox)3] x 0.5 H2O (M(II)M(III) = MnCr, FeCr, CoCr, NiCr, ZnCr, MnFe, FeFe); bpy = 2,2′-bipyridine; ppy = 2-phenylpyridine; ox = Oxalate Dianion. *Inorg. Chem.* **2006**, *45*, 5653−5660.

(30) Nuttall, C. J.; Day, P. The Magnetic Structures of the Layer Ferri- magnets $P(C_6D_5)_4M^{II}Fe(C_2O_4)_3$ (MII = Mn, Fe). *Inorg. Chem.* **1998**, *37*, 3885−3888.

(31) Pellaux, R.; Schmalle, H. W.; Huber, R.; Fischer, P.; Hauss, T.; Ouladdiaf, B.; Decurtins, S. Molecular-Based Magnetism in Bimetallic Two-Dimensional Oxalate-Bridged Networks. An X-ray and Neutron Diffraction Study. *Inorg. Chem.* **1997**, *36*, 2301−2308.

(32) Maczka, M.; Ciupa, A.; Gagor, A.; Sieradzki, A.; Pikul, A.; Ptak, M. Structural, Magnetic and Dielectric Properties of Two Novel Mixed-Valence Iron(II)−Iron(III) Metal Formate Frameworks. *J. Mater. Chem. C* **2016**, *4*, 1186−1193.

DOI: 10.1021/acs.inorgchem.6b01866
Inorg. Chem. XXXX, XXX, XXX−XXX